

Polycapillary optics for soft X-ray imaging and tomography

D. PACELLA⁽¹⁾(*), S. DABAGOV⁽²⁾(³), F. MURTAS⁽²⁾, A. ROMANO⁽¹⁾,
D. HAMPAI⁽²⁾, L. GABELLIERI⁽¹⁾ and D. MAZON⁽⁴⁾

⁽¹⁾ *Euratom-ENEA, C.R. Frascati - Via E. Fermi 45, 00044 Frascati (Rome), Italy*

⁽²⁾ *INFN - Via E. Fermi 40, 00044 Frascati (Rome), Italy*

⁽³⁾ *P.N. Lebedev Physical Institute - Leninsky Pr. 53, 119991 Moscow, Russia*

⁽⁴⁾ *Euratom-CEA, DSM-IRFM - Cadarache, 13108 St Paul lez Durance, France*

(ricevuto il 22 Dicembre 2010; pubblicato online il 22 Settembre 2011)

Summary. — Magnetic plasmas are extended volumetric sources of X-rays, and these emissions could reveal a lot of information about the processes occurring into the plasmas. Unfortunately, the constraints posed by these toroidal devices (high neutron flux, gamma and hard-X background, extremely high radiofrequency powers, high magnetic fields, optical limitations and so on) are very severe and limit strongly the possibility to install X-ray detectors directly into or close to the machine. Soft X-ray diagnostics are meant both as tomography and imaging. We started, therefore, to investigate the feasibility of using polycapillary optics for these purposes, in collaboration between Istituto Nazionale di Fisica Nucleare (INFN)-Frascati, Ente per le Nuove tecnologie, l'Energia e l'Ambiente (ENEA)-Frascati and the Commissariat de l'Energie Atomique (CEA)-Cadarache. The first tests were performed in order to characterize the polycapillary lenses (convergence, divergence, efficiency, spectral dispersion, etc.) for distances much larger than the optical focal length of the lenses, both for the detector and for the source. A silicon-based C-MOS imager (Medipix 2) has been used as a detector and the micro focus X-ray tubes as point-like sources. Results of these preliminary tests are presented, and the imaging capabilities of a polycapillary lens as well.

PACS 41.50.+h – X-ray beams and X-ray optics.

PACS 07.85.-m – X- and γ -ray instruments.

PACS 28.52.Lf – Components and instrumentation.

1. – Introduction

Polycapillary lenses have been studied at the LNF-INFN laboratory for a preliminary characterization, with the aim of using them in soft X-ray (SXR) diagnostics for Magnetic

(*) E-mail: daniilo.pacella@enea.it

Fusion Plasmas. This work is part of a collaboration between LNF-INFN, ENEA-Frascati and CEA-Cadarache in the field of SXR diagnostics and techniques for Nuclear Fusion experiments. The first tests were performed to characterize the polycapillary lenses [1] (convergence, divergence, efficiency, spectral dispersion, aberrations, etc.) in the SXR range 5–25 keV and for distances much larger than the optical focal length of the lenses, both for the detector and the source. A silicon-based C-MOS imager (Medipix 2) has been used to detect the radiation, while as a point-like source we have used the micro focus X-ray tubes.

These optics have been used so far for SXR microanalysis [2-4] to deliver the radiation produced by a tube onto a sample studied, and/or to collect the radiation emitted by the sample (μ -fluorescence, for example) and focus it on a detector. In those studies some features of microimaging by means of polycapillary optical elements were revealed. In these cases, sample or detector are mostly located in the focal points of the lens. Unlikely, the studies discussed in this paper were motivated by the possibility of using the polycapillary optics for X-ray imaging or tomography in Magnetic Controlled Fusion (MCF) [5] for extended sources. Indeed, in the experiments the plasma (X-ray source) is extended (from a few to hundreds cubic meters) and the optics has to be located far from the plasma. Detectors also should be moved as far as possible from the plasma, because of the strong background radiation (neutrons, hard-X, γ) in the vicinity of the plasma [5]. Polycapillary optics offers, therefore, a potential advantage both to be highly selective only for SXR radiation and of transporting it far from the plasma.

2. – Laboratory set-up

An experimental setup with a cabinet and an optical table was designed and developed specially for R&D of X-ray optical systems at Laboratori Nazionali di Frascati (LNF) [6]. The radiation sources are two: 50 W Cu or Mo X-ray tube (Oxford Apogee 5000) with a source spot size of about 50 μm . There are three different detector units available: a scintillator with an effective working area of about 1 in^2 for the alignment of polycapillary lens together with X-ray source; a Silicon Drift Detector (SDD) with a 30 mm^2 working area for the measurements of the spectra, and finally a C-MOS imager (Medipix 2) as 2D detector [7]. The microchip, working in photon counting mode, has been designed at CERN following the parameters defined by the Medipix Collaboration. The detector is formed by a pixellated 300 μm thick silicon sensor. The chip performs single photon counting in each pixel cell. The pixel size is $55 \times 55 \mu\text{m}^2$, forming an array of 256 by 256 pixels, whose active area is $1.4 \times 1.4 \text{ cm}^2$. Each pixel is bump-bonded to the corresponding channel of the chip, providing the analog and digital treatments of the signal [8].

3. – Characterization of polycapillary lenses

The full lens has been characterized by using an electronic tube with a Mo anode powered at 25 kV, 150 μA (continuous spectra with the K_α line of Mo at 17.4 keV in addition), while the half lens by an X-ray tube with a Cu anode and a Ni filter (K_α line of Cu at 8.04 keV), powered at 15 kV, 300 μA . The images have been acquired with the Medipix 2 [8]. Full and half lens have been characterized to study their properties at large distances compared with the focal distances. In particular, the output focus of the full lens has been found by a scan of the detector-lens distance, as shown in fig. 1.

The intensity of the spot is found to be fairly Gaussian. We adopted therefore the half width at half maximum (labelled sigma in the plots) as measurement of the cross

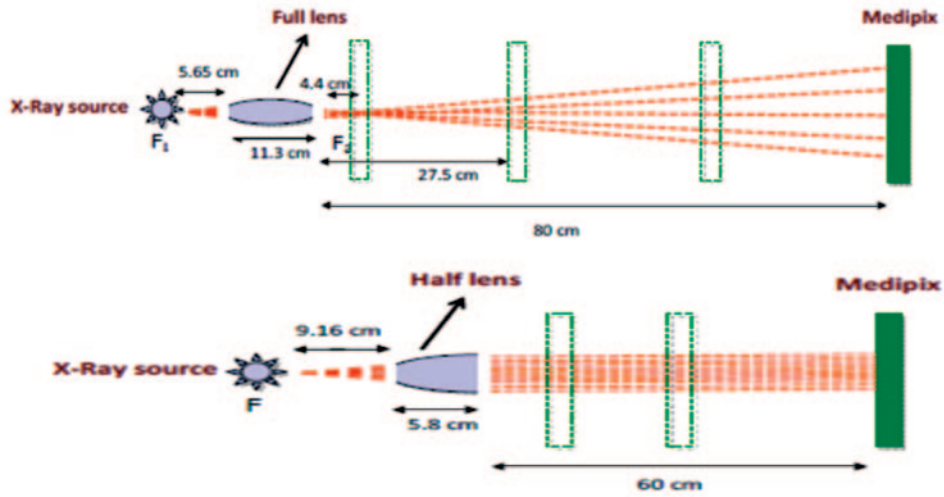


Fig. 1. – Top: Layout for the measurement of divergency of the full lens. Bottom: Layout for the measurement of divergency of the half lens.

dimensions of the beam. The values of sigma along the two directions (x and y) perpendicular to the optical axis (z) are plotted in fig. 2, for the full lens. Sigma is given in units of pixel ($55 \mu\text{m}$). We can observe how good is the geometrical propagation of the Gaussian beam at distances (60 cm) much larger than the focal distance (4.4 cm). The spot broadening is indeed linear with the distance; the total geometry divergence results equal approximately to 2.6 degree, with a small difference in x - and y -axis, like a sort of weak astigmatic aberration. The same measurement has been done with the half lens (see layout in fig. 1 (bottom)). In this case the output beam is almost parallel even at long distances (see fig. 2, right). It shows a very weak convergence up to 22 cm and then

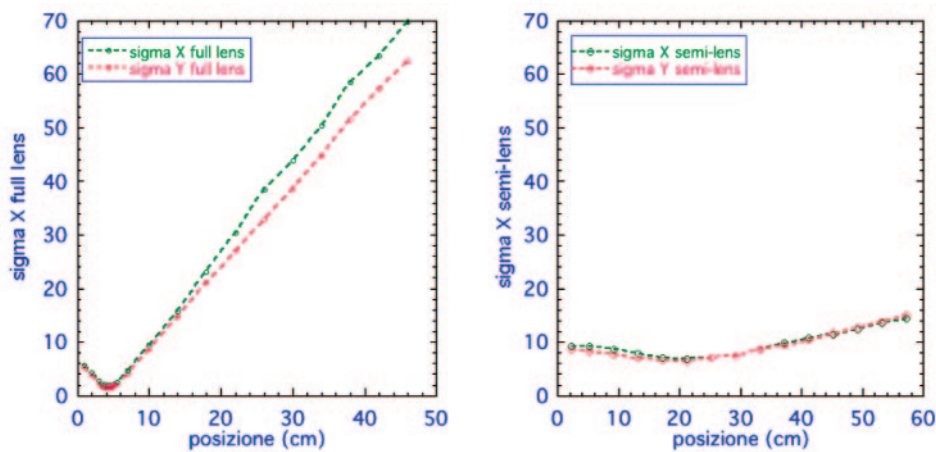


Fig. 2. – Left: Divergence of the full lens, in the directions perpendicular to the optical axis (z). Right: Quasi-parallelism of the half lens, in the directions perpendicular to the optical axis (z).

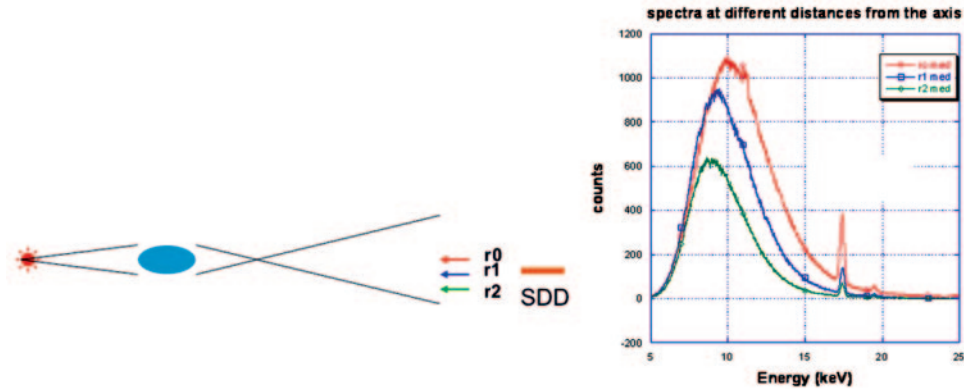


Fig. 3. – Left: Schematic view of the measurements of the spectra at three radial positions. Right: Spectra at different distances from the optical axis.

a slight divergence of about 0.3 degree. The beam at 60 cm is only 40% wider than at the exit of the lens.

For both lenses the exit beam has a spatial distribution almost Gaussian, while the intensity of the beam at the optics entrance is fairly uniform. This is an expected feature of these lenses, because the effective working area of each capillary (as its acceptance angle) reduces moving from the axis outward; this is due to the increasing curvature of the capillaries from the axis to the periphery. This effect can be quantified with a transmission function $T(r)$, where r is the radial coordinate from the optical axis to the edge of the lens, in a cylindrical geometry. Once this function is carefully measured, it can be used to correct the output intensity. In order to see if this reduction of the transmission efficiency towards the edge depends on the energy of the X-ray radiation, we measured the spectra at three radial positions (see fig. 3 left), with a SDD. Spectra are shown in fig. 3 (right) where the decrease of intensity towards the periphery is confirmed. But it is progressively stronger at higher energies, as shown in fig. 4 where the ratio of intensity of the two radial positions $T(r_2)/T(r_1)$ is plotted *vs.* energy. This sort of chromatic aberration is clearly explained by the fact that the effective area of the peripheral capillaries reduces for X-ray photons of higher energy.

4. – Imaging properties

The imaging with the use of lens for various samples (needle, wire, mesh, etc.) has been done with a full lens using the X-ray tube with a Mo anode: voltage and current have been set at 25 kV and 150 μ A, respectively. A radiography of the sample (mask) has been done at first, putting it just in front of the detector, to check structure, contrast and dimensions and so on, as a reference. The image through the lens is obtained placing the sample (mask) just before (roughly 5 mm) the optics.

In fig. 5 (left) the radiography of the needle is shown, while in fig. 5 (right) the imaging of the needle through the lens is presented, with a magnification $M = 2.8$. The needle in this second case is rotated because of mechanical constraint of the supports. Following these encouraging preliminary results, a plastic foil with holes of about 400 μ m has been used (see its radiography in the left fig. 5) to test the imaging proprieties of the full

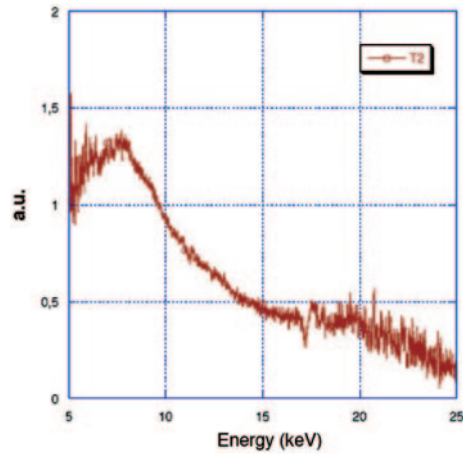


Fig. 4. – Relative transmission $T(r_2)/T(r_0)$ vs. energy.

lens at higher resolution. Apart from the bright small spots in correspondence of the holes, there is also a larger circular spot in the centre of the image because the plastic foil is not fully opaque to this X-ray spectrum. In fig. 6 (right), we can observe that the geometrical shape (the silhouette) of this sample is perfectly reproduced. There is only a decrease of the intensity at the edges of the lens but it could be corrected by using an appropriate factor. Finally a rectangular mesh made of nickel wires of $100\ \mu\text{m}$ diameter and pitch $1.3\ \text{mm}$ has been used (see radiography in fig. 7 (left)). The image produced by the lens (see fig. 7, right) shows only two wires in horizontal direction since the size of the pitch ($\sim 1.3\ \text{mm}$) is only slightly smaller than the diameter of the lens ($\sim 4\ \text{mm}$).

In fig. 8 intensity along the vertical direction (dark arrow) is plotted. It is possible to see a drop of intensity compared to the background line (found without the grid) in correspondence of the wire. This drop is not rectangular because the wire does not show the same thickness to the X-ray flux. The thickness is roughly constant only in the central part of the wire ($\Delta x \sim 40\ \mu\text{m}$ wide). We found therefore a resolving power

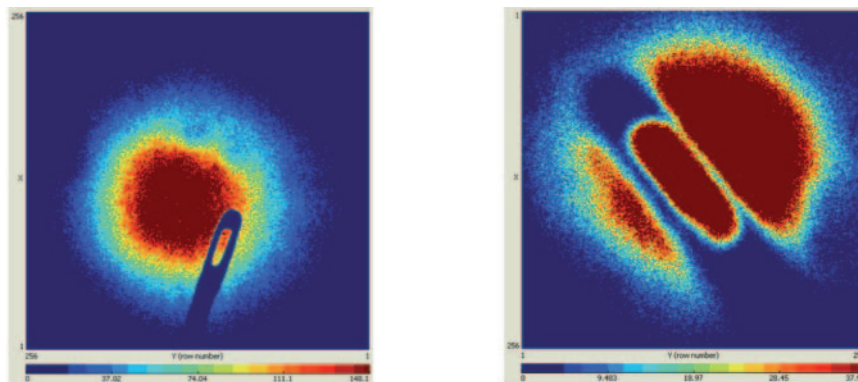


Fig. 5. – Left: Radiography of a needle. Right: Image of the needle with the full lens.

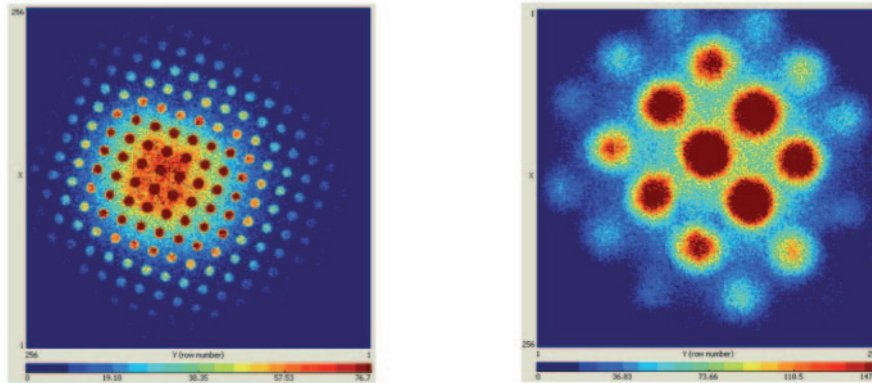


Fig. 6. – Left: Radiography of a plastic foil with holes. Right: Image with a full lens of a plastic foil with holes.

($d/\Delta x$) of about $4\text{ mm}/40\ \mu\text{m} = 100$, where d is the diameter of the lens. Images of the plastic foil with holes have been done with different magnifications, moving the detector from 12 cm to 32 cm far from the lens. The quality of the image is pretty good in all the positions, except in approaching of course the focus. The imaging properties have been also tested for half-lens, by using the plastic foil with holes of $400\ \mu\text{m}$, with the X-ray tube with a Cu anode at 15 kV and current of $300\ \mu\text{A}$. The source is in the focus lens and the mask just before the lens. The imaging properties have been explored by putting the detector in two positions, one just at the exit of the lens (see fig. 9, left) and the other one at large distance, about 60 cm (see fig. 9, right). In the position close to the lens the image is preserved, while it is lost when we move the detector far away, producing a very precise circular spot. This result is expected, because the divergence of each individual polycapillary (0.22 degree at about 8 keV of the Cu line) becomes comparable or even greater than the very weak geometrical divergence (0.17 degree) of the half lens.

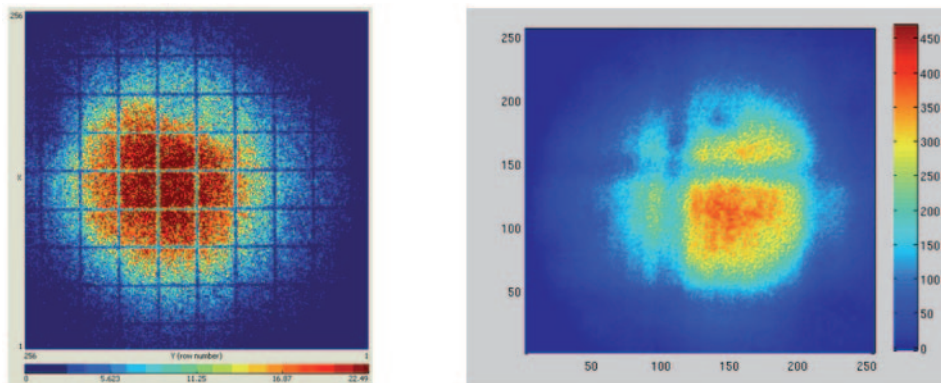


Fig. 7. – Left: Radiography of a metallic mesh of Ni wires. Right: Image with the full lens of a metallic mesh of Ni wires.

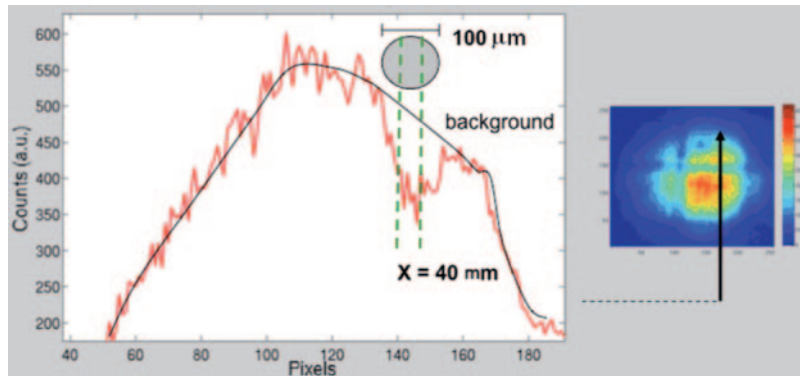


Fig. 8. – Intensity along the vertical direction (dark arrow) of the wire image.

5. – Polycapillary optics for imaging and tomography in MCF

The results discussed in the previous section confirm the potentialities of polycapillaries as optics for imaging and/or tomography in Magnetic Confined Fusion [9, 10]. These plasmas have central temperatures from a few to tens of keV, being only a few tens of eV at the edge; most of the plasma emits therefore strongly in SXR range [11, 12]. Since the power densities at stake in the fusion experiments are of the order of magnitude of MW/m^3 , the SXR emissions are very intense, in the range 10^{16} – 10^{18} $\text{ph}/(\text{s m}^3 \text{sr})$. Polycapillaries offer many advantages when compared with the pinhole, the most used optical component in MCF. Since the etendue of an optic, in the limit of sources at large distances, is given by the product of the active area and the entrance angle, we realize immediately how different are these two kinds of optics. First of all polycapillaries are extremely selective for the X-ray band which they are optimized for. Second, they have a smaller entrance angle, so the line of sight is much more defined, without losing luminosity because compensated by the active area of the lens, much higher than for pinhole. Polycapillaries (half lens, full lens, cylindrical lens) offer a large flexibility in designing optical systems to get the radiation from the plasma. Full lens, with an entrance angle of

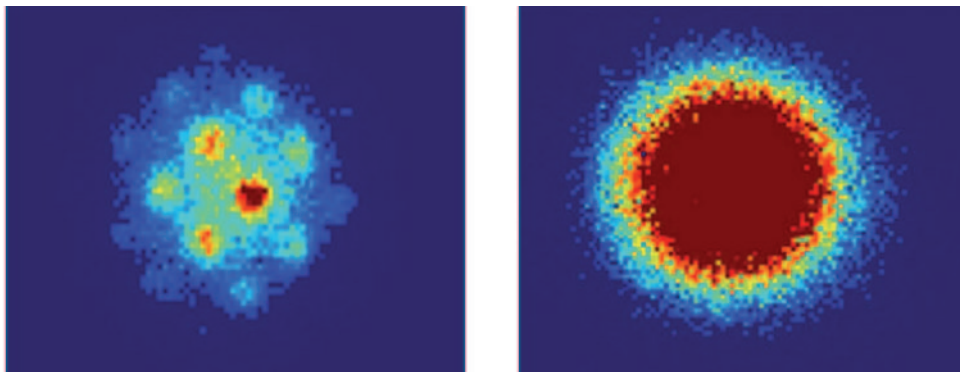


Fig. 9. – Left: Image with an half lens just after the lens. Right: Image with an half lens at large distance (60 cm) from the lens.

a few degrees and located at meters far from the source, allows 2D imaging of portions of the entire plasma. Half lens allows the collection of radiation from a larger geometrical entrance cone (aperture of a few degrees), while the cylindrical lens gather radiation from a well defined line of sight, having a divergence of only a few milliradians. These lenses in particular could be thought for a tomography array. Cylindrical lenses with large area (dia ~ 5 mm) offer a greater luminosity, while long and thin cylindrical lenses (dia < 1 mm) could be bent to form a fan-in or fan-out array. Half and cylindrical lenses produce an almost parallel output beam (0.17 degree), with the advantage to move the detector far away, even at meters of distance. Full lens produces a divergent beam, with an image magnification, that offers the advantage, if useful, of using large-area detectors, placed at large distances.

6. – Conclusions

Imaging properties have been demonstrated for full lens, with a resolving power at least of about 100 and for distances much longer (15 times) than the focal distance. Efficiency is found progressively lower at the edge, as expected, and dependent on the energy of the X-ray photons. Half-lens revealed an excellent light collector, having an output beam with a very low divergence (quasi-parallel). Cylindrical lenses, with large or very small active area, could be used in tomography arrays. Thanks to these optics, the detector can be moved far from the lens and the background suppression enhanced. All that is particularly valuable in case of Magnetic Fusion, due to the harsh radiative environmental conditions.

REFERENCES

- [1] DABAGOV S., *Phys. Usp.*, **46** (2003) 1053.
- [2] SCHIELDS P. J. *et al.*, *Powder Diffr.*, **17** (2002) 70.
- [3] HAMPAI D. *et al.*, *Opt. Lett.*, **33** (2008) 2743.
- [4] HAMPAI D. *et al.*, *Nucl. Instrum. Methods B*, **244** (2006) 481.
- [5] WESSON J., *Tokamaks* (Oxford University Press) 2004.
- [6] CAPPUCIO G. *et al.*, *LNF Activity Report 2004* (2004) p. 181; www.lnf.infn.it/rapatt.
- [7] LLOPART X. *et al.*, *IEEE Trans. Nucl. Sci.*, **49** (2002) 2279.
- [8] DAVIDSON D. W. *et al.*, *IEEE Trans. Nucl. Sci.*, **50** (2003) 1659.
- [9] A.A. V.V., *Progress in the ITER Phys. Basis Nucl. Fus.*, **47** (2007).
- [10] DONNE A. J. H., *Trans. Fusion Sci. Technol.*, **53** (2008) 379.
- [11] PACELLA D. *et al.*, *Rev. Sci. Instrum.*, **72** (2001) 1372.
- [12] DE MICHELIS C. and MATTIOLI M., *Nucl. Fus.*, **21** (1981) 677.